

# Aerial image based lens metrology for wafer steppers

Peter Dirksen<sup>a</sup>, Joseph J.M. Braat<sup>b</sup>, Augustus J.E.M. Janssen<sup>c</sup>, Ad Leeuwestein<sup>c</sup>, Tomoyuki Matsuyama<sup>d</sup>, Tomoya Noda<sup>d</sup>

<sup>a</sup>Philips Research Europe, Belgium

<sup>b</sup>Delft University of Technology, The Netherlands

<sup>c</sup>Philips Research Europe, The Netherlands

<sup>d</sup>Nikon Corporation, Japan

## ABSTRACT

Phase Measurement Interferometers (PMI) are widely used during the manufacturing process of high quality lenses. Although they have an excellent reproducibility and sensitivity, the set-up is expensive and the accuracy of the measurement needs to be checked frequently.

This paper discusses an alternative lens metrology method that is based on an aerial image measurement. We discuss the Extended Nijboer-Zernike (ENZ) method and its application to aberration measurement of a high-NA optical system of a wafer stepper. ENZ is based on the observation of the through-focus intensity point-spread function of the projection lens. The advantage of ENZ is a simple set-up that is easy to run and maintain and provides good accuracy. Therefore the method is useful during lens assembly in the factory.

The mathematical framework of ENZ is shown and the experimental procedure to extract aberrations for a high-NA lens is demonstrated on a high-NA DUV lithographic lens. PMI data is given as reference data. It is shown that ENZ provides an attractive alternative to the interferometer.

**Keywords:** Optical lithography, aberrations, PMI, Extended Nijboer-Zernike theory.

## 1. INTRODUCTION

Modern lithographic projection lenses have a nearly ideal wavefront with typical wavefront errors below  $10m\lambda$ . This amazing result is achieved by continuous improvement of the lens design, optical materials, lens metrology and by using advanced polishing techniques.<sup>1</sup> During the adjustment phase, lens metrology plays a crucial role as it is part of the feedback loop that determines the relative position of the various lens elements. The metrology tool of choice is a phase measurement interferometer (PMI). The PMI measures the key parameters of the lens: the wavefront aberrations, usually expressed in Zernike coefficients. During lens assembly the wavefront is optimized to the lowest possible level.

The PMI measures effectively an optical phase difference between the wavefront of the projection lens and the wavefront of a reference surface. After careful calibration and adjustment of the interferometer set-up, the wavefront of the projection lens is extracted. Nikon uses a so-called Fizeau type interferometer, where the reference surface is a spherical mirror. This system achieves a very high accuracy and reproducibility, viz. better than  $\lambda/1000$  or  $1m\lambda$ .

The Extended Nijboer-Zernike (ENZ) method is an alternative lens metrology method. The ENZ-method is based on aerial image measurements, i.e. the observation and analysis of the through-focus intensity point-spread function. The ENZ-method is self calibrating and uses no reference surface. The ENZ-method retrieves not only the phase errors but also the transmission errors of the lens. The method is well adapted for optical systems

---

Further author information: (Send correspondence to peter.dirksen@philips.com)

PD: Philips Research Europe, Kapeldreef 75, B-3001 Leuven, Belgium

JJMB: Optics Research Group, Faculty of Applied Sciences, Delft University of Technology, Lorentzweg 1, NL-2628 CJ Delft, The Netherlands

AJEMJ and AL: Philips Research Europe, NL-5656 AA Eindhoven, The Netherlands

TM and TN: Nikon Corporation, 201-9 Miizugahara, Kumagaya City, Saitama, Japan

with relative large chromatic errors and does not require a coherent source. ENZ achieves a reproducibility of about  $1m\lambda$ . The ENZ-method is not only applicable to low-and-medium-NA lenses, but can be used for very high-NA lenses<sup>2,3</sup> as well.

This paper compares the two measurement methods for lens metrology: PMI and ENZ. Measurement results are shown for a prototype DUV lens with an NA of 0.75. The lens discussed shows significant aberrations and does not represent the current state of art. This lens is selected for the purpose of demonstration of the measurement capability of the two methods only.

The paper is organized as follows. Section 2 discusses the basic principles of the PMI. Section 3 discusses the ENZ-theory and the experimental set-up used to measure the aerial image of a lithographic lens. Section 4 shows samples of the experimental through-focus intensity point-spread function and the retrieval of phase and transmission errors. The PMI results are compared to the ENZ results for the prototype lens. We discuss a reticle adjustment experiment, where spherical aberration is introduced in a controlled way. It is shown that the ENZ-method tracks the aberration changes well and is able to optimize the reticle position to a low level of spherical aberration. Section 5 gives a summary. Finally, the appendix shows some of the mathematical framework of the ENZ-method.

## 2. PHASE MEASUREMENT INTERFEROMETER

During assembly and testing of lithographic projection lenses, Nikon uses a so-called Fizeau type of interferometer. Figure 1 shows the basic set-up. The incoming light rays are partly reflected on the Fizeau surface and form

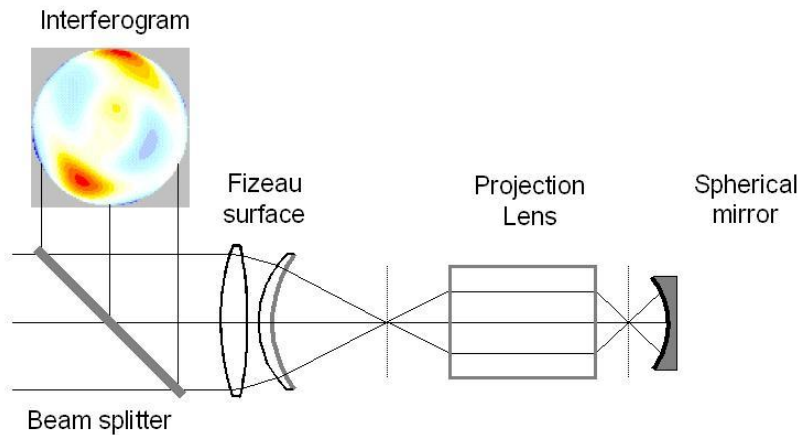


**Figure 1.** Nikon uses a so-called Fizeau type interferometer. The incoming light rays are partly reflected on the Fizeau surface. The transmitted rays pass the projection lens, are reflected by the spherical mirror and pass the projection lens again. Eventually the rays interfere and form an interferogram.

the reference rays. The transmitted rays pass the projection lens, are reflected by the spherical mirror and pass the projection lens again along the same route. Eventually they are reflected by the beam splitter and interfere with the reference ray to form the interferogram. The light source of the Fizeau interferometer is a narrow band, mono-mode laser with a coherence length exceeding at least three times the track length of the projection lens.

The interferogram represents the combined wavefront error  $W$  of the projection lens and spherical mirror:

$$W = W_{\text{Spherical mirror}} + 2 \cdot W_{\text{Projection lens}} \quad (1)$$

The non-rotationally symmetrical wavefront errors of the mirror can be determined by a calibration procedure, but the spherical errors are assumed to be known from the mirror design. In order to extract the projection lens aberrations, the wavefront of the mirror is removed from the measurement. In principle, the Fizeau surface also

has a small contribution to the wavefront, but is neglected here. The advantage of the Fizeau interferometer is its stability and very high accuracy and reproducibility.

In this paper we represent the phase aberrations using both the Born and Wolf convention and the fringe convention for the Zernike terms:

Zernike term			
$(n, m)$	Name	$R_n^m(\rho)\cos(m\theta)$	Term
(0,0)	Piston	1	$Z_1$
(1,1)	Tilt	$\rho \cos(\theta)$	$Z_2$
(2,0)	Defocus	$2\rho^2 - 1$	$Z_4$
(2,2)	Astigmatism	$\rho^2 \cos(2\theta)$	$Z_5$
(4,0)	Spherical	$6\rho^4 - 6\rho^2 + 1$	$Z_9$
(3,1)	X-Coma	$(3\rho^3 - 2\rho) \cos(\theta)$	$Z_7$
(3,3)	X-Three point	$\rho^3 \cos(3\theta)$	$Z_{10}$

⋮

### 3. FROM AERIAL IMAGE TO WAVEFRONT

An alternative method to obtain the wavefront errors of an optical system is an aerial measurement of the intensity point-spread function. This method is well adapted for optical systems with relatively large chromatic errors and does not require a coherent source. There are a number of algorithms to extract the wavefront errors, such as the Gerchberg-Saxton method.<sup>4-7</sup> However, the stability is not always guaranteed and these methods tend to be sensitive to noise. We propose an alternative method that is more practical and easily adapted to the quality measurement of projection lenses. For analysis we use the so-called Extended Nijboer-Zernike (ENZ) method. The ENZ-method is based on the analysis of the through-focus intensity point-spread function.

Aberration retrieval of a projection lens basically involves three steps. Figure 2, shows the aerial image measurement set-up during the measurement phase. A  $\lambda = 248nm$ , NA=0.75 lithographic projection lens with a 4X reduction ratio is mounted in the set-up. A test reticle with a pinhole is at the low-NA side in the reticle plane. The pinhole diameter of  $0.1 \mu m$  is small compared to the resolution of the lens. An intermediate image is formed at the wafer level. The objective lens, with an NA=0.78, is stepped through focus. The image of the pinhole, as recorded by the CCD-camera, represents the point-spread functions of the combined projection lens and objective lens system.

Figure 3, shows the set-up during the calibration phase. Now the pinhole reticle is in the wafer plane and the image of the pinhole, as recorded by the CCD-camera, represents the point-spread function of the objective lens. Again the objective lens is stepped through focus and records the through-focus PSF of the objective lens. Note that this calibration step has to be performed only once.

Finally, the through-focus intensity point-spread functions are analyzed using the ENZ-method and the wavefront of the projection-lens objective-lens combination and the wavefront of the objective lens are obtained. These two wavefronts are subtracted from each other and thus the wavefront of the projection lens is obtained.

#### 3.1. Basic expressions used in the Extended Nijboer-Zernike theory

Below we briefly review the Extended Nijboer-Zernike theory to calculate the intensity point-spread function and indicate how to obtain the transmission and phase aberrations. The point-spread function or impulse response<sup>8</sup> of an optical system is the image of an infinitely small object. In practice, an object having a diameter of the order  $\sim \frac{\lambda}{2NA}$  is a fair approximation. The finite hole size is taken into account. The complex amplitude of the point-spread function is denoted as  $U(x, y)$ , with  $(x, y)$  the coordinates scaled to the ratio of wavelength and numerical aperture.

We write the pupil function as:

$$A(\rho, \theta) \cdot \exp\{i\Phi(\rho, \theta)\} = \sum_{n,m} \beta_{n,m} Z_n^m(\rho, \theta), \tag{2}$$

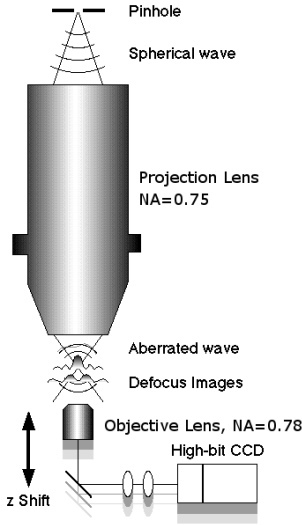


**Figure 2.** During the measurement phase, the pinhole is at the low-NA side. An intermediate image is formed at the wafer level. The image at the CCD-camera represents the point-spread function of the combination of projection lens and objective lens.

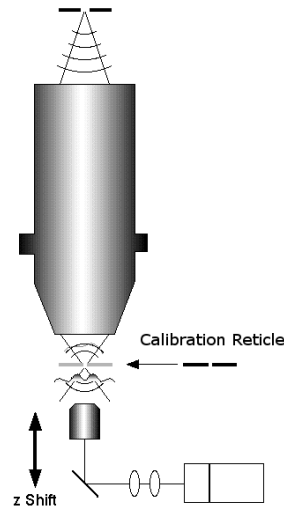


**Figure 3.** During the calibration phase, the pinhole is at the wafer level. The image at the CCD-camera represents the point-spread of the objective lens only.

with  $A$  the amplitude pupil transmission function and  $\Phi$  the pupil phase function and  $Z_n^m(\rho, \theta)$  the Zernike terms with coefficients  $\beta_{n,m}$ . According to the ENZ-theory:

$$I \approx 4\beta_{0,0}^2 |V_0^0|^2 + \beta_{0,0} \sum_{(n,m) \neq 0} (\text{Im}(\beta_{n,m}) \Psi_n^m + \text{Re}(\beta_{n,m}) \chi_n^m) \cos(m\phi), \quad (3)$$

where the intensity is written as a linear summation of basic functions  $\chi_n^m, \Psi_n^m$ . We assumed that  $\beta_{0,0}$  is real and positive and "relatively" large compared to the totality of all other  $\beta$ 's. For small aberrations the  $\chi_n^m$  terms correspond to the phase errors and the  $\Psi_n^m$  terms correspond to the amplitude errors. The projection lens aberrations manifest themselves as coefficients  $\beta_{n,m}$  of the basic functions:

$$\begin{aligned} \chi_n^m(r, f) &= \gamma_m \text{Re}\{i^m V_0^{0*} V_n^m\} \\ \Psi_n^m(r, f) &= \gamma_m \text{Re}\{i^{m+1} V_0^{0*} V_n^m\}, \end{aligned} \quad (4)$$

with  $\gamma_m = 4$ ,  $m = 1, 2, \dots$ ,  $\gamma_0 = 8$ . Appendix A gives the definitions of the scaled coordinates as well as the definition of the functions  $V_n^m(r, f)$  for the low-NA case.

In solving the aberrations from the measured point-spread function, the key step, see Eq.3, is to linearize the theoretical intensity, comprising the  $\beta$ s as unknowns, by deleting second-order terms, and to optimize the match between the linearized, theoretical intensity and the given intensity in the focal region. This approach is valid for a good lens, having small transmission variations and phase errors ( $A \approx 1$  and  $|\Phi| \ll 1$ ) only.

### 3.2. Retrieving large wavefront errors: the Predictor-Corrector approach

For general pupil functions that may contain amplitude errors or larger pure-phase aberrations, the linearization error(s) cannot be ignored. By adopting a predictor-corrector approach, the effect of linearization can be eliminated iteratively and this yields accurate or even perfect retrieval of aberrations well beyond the diffraction limit. This approach is described in detail in Ref.<sup>9</sup> Figure 4 shows the convergence of the aberration-free term or  $\beta_{0,0}$ -coefficient. Already after a few iterations the convergence is better than  $10^{-5}$ . The outcome of the predictor-corrector procedure is an accurate estimate of the  $\beta$ - coefficients. Finally, using equation Eq. 2, the transmission error  $A(\rho, \theta)$  and phase error  $\Phi(\rho, \theta)$  are obtained from the same experiment.

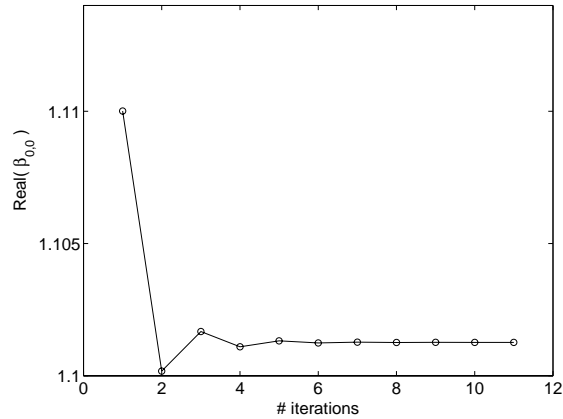


**Figure 4.** Predictor - corrector is an iterative procedure to eliminate the effect of linearization. This procedure is used to retrieve large aberrations, well beyond the diffraction limit. The graph shows the convergence of the aberration free coefficient  $\beta_{0,0}$  towards the value 1.1013. A few iterations are sufficient to achieve a good convergence better than  $10^{-5}$ .

### 3.3. Accounting for chromatic aberrations

For certain projection lenses it is important to account for the chromatic aberrations. This is especially important if a source with a relatively large bandwidth is used, for example when a Mercury arc-lamp is used in combination with an I-line projection lens. A similar situation may occur for DUV lenses or 193 nm systems. Although these lenses use a coherent laser source, their chromatic errors are much larger.

The effects of the chromatic errors is a stochastic variation of the focus position and thus an image blur in the vertical direction. The magnitude depends on the chromatic error and the bandwidth of the light source. To a good approximation:

$$\sigma_F \approx C_c \Delta\lambda, \quad (5)$$

where  $\sigma_F$  is the standard deviations of the focus position, the coefficient  $C_c$  represents the chromatic error of the projection lens and  $\Delta\lambda$  represents the standard deviation of the source wavelength distribution.

The ENZ-method accounts for the chromatic errors by modifying the basic functions. The formulas that arise are analytical in nature and are especially useful for the case of a small-to-medium-large value of the blur parameter. By way of illustration, we present the first-order corrected expression for the dominant aberration-free term,  $|V_0^0|^2$ . It is given as

$$I(r, f) = |V_0^0|^2 - \frac{1}{2}\sigma_F^2 \left[ \frac{1}{6}|V_0^0|^2 - \frac{1}{2}|V_2^0|^2 + \frac{1}{6}V_0^0V_4^{0*} + \frac{1}{6}V_4^0V_0^{0*} \right]. \quad (6)$$

Here we only reproduce the first order correction for a stochastic focus variation, but a more general approach including the effects of image blur in the horizontal plane and full second order corrections can be found in Ref.<sup>10</sup> The standard deviation  $\sigma_F$  is determined directly from the intensity PSF and does not require an additional experiment.

Similar to the case without chromatic errors, the intensity is written as a linear summation of basic functions  $\chi_n^m, \Psi_n^m$ , with coefficients  $\beta_{n,m}$  now representing the wavelength averaged aberrations. Thus, the ENZ-method directly determines the wavelength averaged aberrations, which are the relevant parameters for the imaging performance of the lens.

### 3.4. The impact of transmission errors

Pupil transmission errors are often ignored in the discussion on lens quality. Nevertheless transmission errors can impact the lens performance and contribute to across-the-field linewidth variations in a similar way as phase

errors do. As potential causes for transmission errors we mention an obstruction, a bad anti-reflection coating or contamination of a lens element.

A simulated example of the impact of a transmission error is shown in Fig. 5. Here we assumed a transmission error of the form:

$$A(\rho) = 1 - 0.10\rho^2 \cos(2\phi) \tag{7}$$

In our example, the mask is a binary mask with a 90 nm line. We vary the space from fairly isolated to fully dense. The optical system has a wavelength of  $\lambda = 0.193\text{nm}$  and  $\text{NA}=0.80$ . We assumed a conventional illumination with a coherence value of 0.5. Figure 5 compares the simulated proximity curve for horizontal and vertical lines. We observe an impact on the horizontal-vertical linewidth difference of the order of  $\pm 5$  nm. The impact depends on

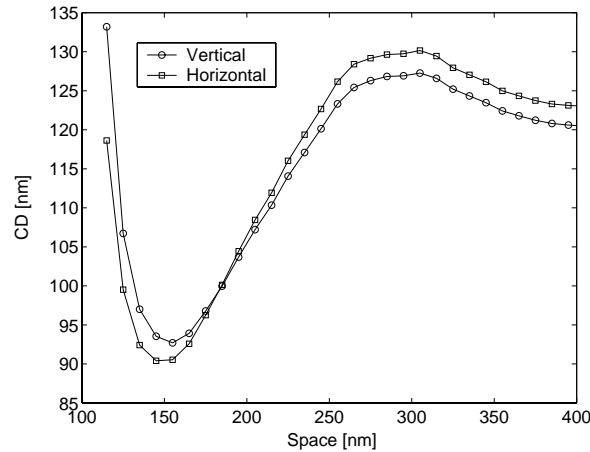


**Figure 5.** The simulated impact of pupil transmission errors on a proximity curve. A transmission error of the form  $A(\rho) = 1 - 0.1\rho^2 \cos(2\phi)$  causes a significant horizontal-vertical linewidth differences.

the feature size, feature orientation, mask type and illumination condition. In our example the transmission error cause HV-linewidth differences and also elliptically deformed contacts, similar to phase-astigmatism. However, unlike astigmatism, the pattern deformation is also present in best focus.

## 4. EXPERIMENTAL RESULTS

### 4.1. Comparing the PMI and ENZ-method

The experimental set-up is described in Sections 2 and 3. In this subsection we compare the results obtained by the PMI and ENZ-set-up. Both set-ups use the same prototype  $\text{NA}=0.75$  DUV-lens.

Figure 6 shows an example of a recorded through-focus intensity point-spread function. Using the ENZ-analysis, as described in 3.1, we determine the  $\beta$ -coefficients. The figure shows a comparison between the raw aerial images (solid lines) and aerial image calculated from the retrieved aberrations (dashed lines). A good match is obtained, with a standard deviation  $1\sigma \sim 0.5\%$ .

The ENZ-method determines the general pupil function in terms of  $\beta$ -coefficients. For small aberrations, the imaginary part of the  $\beta$ -coefficients correspond to phase errors and the real part of the  $\beta$ -coefficients correspond to the amplitude errors. For larger errors, we evaluate Eq. 2 and use the predictor-corrector approach to obtain the phase errors  $\Phi(\rho, \theta)$  as well as the transmission errors  $A(\rho, \theta)$  of the projection lens. An experimental example is shown in Fig. 7.

In an other experiment we compare the results of the PMI to that of the ENZ-method. The results are shown in Fig. 8. The standard deviation between the PMI and ENZ-method is  $1\sigma = 4.6m\lambda$ . The largest deviations between the PMI and ENZ-measurements are observed for the spherical aberration terms. The agreement for the non-spherical terms like coma and astigmatism is better than  $1\sigma = 3m\lambda$ .

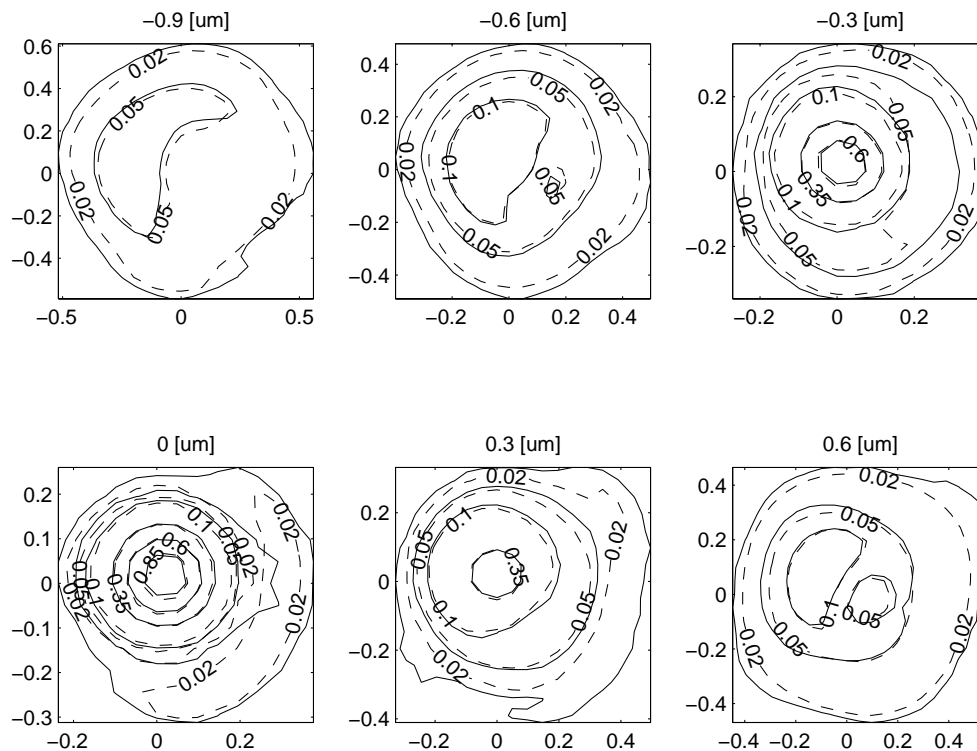


**Figure 6.** A comparison between the raw aerial image data (solid lines) and aerial image calculated from the retrieved aberrations (dashed lines). A good match is obtained, with a standard deviation  $1\sigma \sim 0.5\%$ .

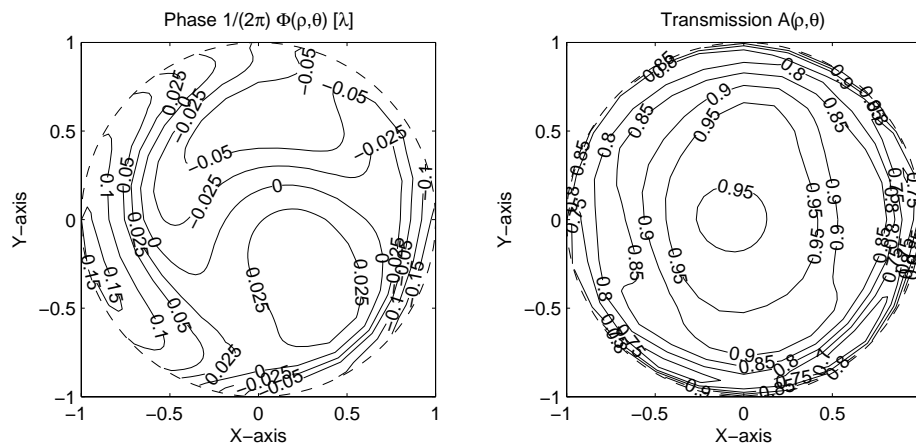


**Figure 7.** ENZ-method retrieves not only the phase errors (left) but also the transmission errors (right) of the lens.

## 4.2. Spherical aberration

As potential causes for errors in the measurement of spherical aberration we mention the exposure wavelength, barometric pressure, the shape of the spherical reference mirror and the shape of the Fizeau surface that all could produce a spherical offset. Another cause is related to the ENZ-method. The intensity point-spread function is recorded through focus, i.e., at a number of discrete focus position. An error in the focus readings would impact the analysis of spherical aberration. Also a DC-offset in the CCD-camera contributes to the spherical terms.

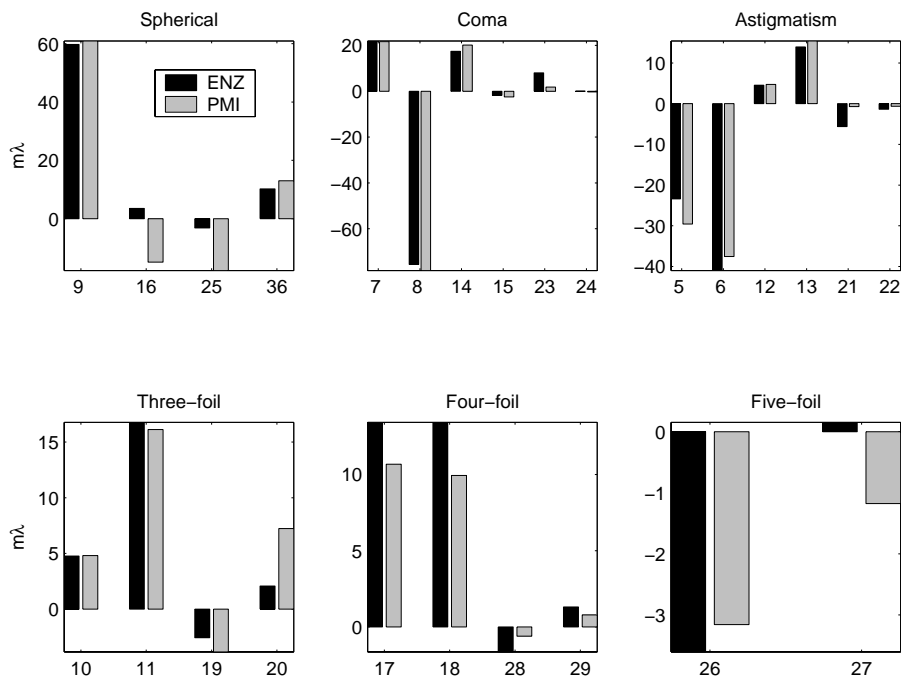


**Figure 8.** A comparison of the Zernike coefficients obtained by the PMI and ENZ-method.

With careful calibration procedures, these errors can be prevented.

A third cause is a change in conjugates, i.e. the exact reticle table and wafer table z-positions have an impact on the spherical terms. We investigated this cause in some detail in a reticle table height detuning experiment. When the reticle table deviates from its nominal position, spherical aberration will be introduced. For an ideal system the dependence of low and high order spherical aberration versus reticle table height is linear and the curves intersect each other at one reticle table height, the nominal position:

$$\begin{aligned} Z_9 &= c_9 \cdot z \\ Z_{16} &= c_{16} \cdot z \end{aligned} \quad (8)$$

At the nominal position, all spherical terms are zero.

Figure 9 shows the results of the reticle table detuning experiment, where the reticle table height is varied from -100 to +100  $\mu\text{m}$  around the nominal position in 11 steps of 20 micron. At each reticle z-position the through-focus intensity point-spread function is recorded and the aberrations are determined. Indeed a sweet-spot is found with spherical terms below  $< 5m\lambda$ . The common crossing point of  $Z_9$  and  $Z_{16}$  is close to the nominal reticle position. We conclude that both the PMI and the ENZ-method have a small spherical offset below  $< 5m\lambda$ . The observed linearity also proves the capability of the predictor-corrector iterative approach to deal with large aberrations.

The experimentally obtained slope (ENZ) and a numerically calculated slope using a ray-trace method are summarized in the table below:

Reticle detuning experiment		
Spherical term	ENZ [ $m\lambda/\mu\text{m}$ ]	Ray-trace [ $m\lambda/\mu\text{m}$ ]
$c_9 = \Delta Z_9/\Delta z$	2.01	2.29
$c_{16} = \Delta Z_{16}/\Delta z$	0.35	0.29

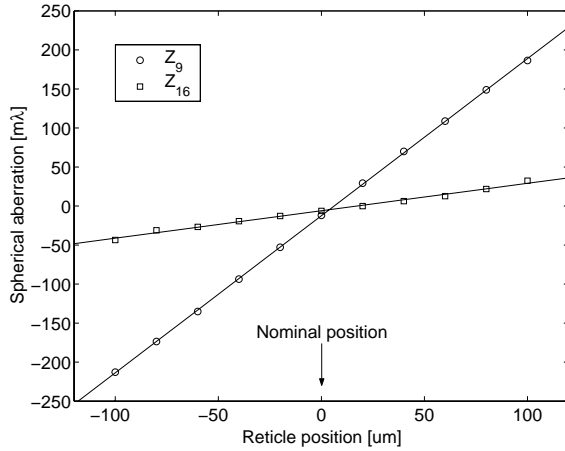


**Figure 9.** The reticle detuning experiment. The spherical aberration coefficients change linearly with the reticle table position. Near the nominal position we find a sweet spot where the spherical aberration coefficients are below  $5m\lambda$ .

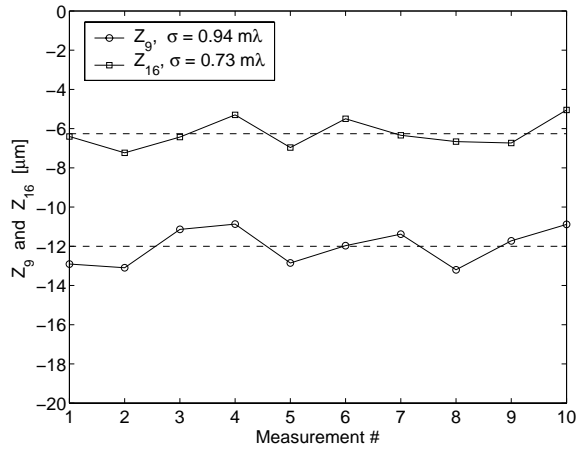


**Figure 10.** At the nominal reticle position, the ENZ-measurement was repeated 10 times. The reproducibility of  $Z_9$  and  $Z_{16}$  is better than  $1m\lambda$ .

Other Zernikes coefficients are found to be virtually independent of reticle table height, which is in agreement with the theory.

At the nominal reticle position, the measurement was repeated 10 times. As an example, Fig. 10 shows the reproducibility measurement and we found a standard deviation of  $1\sigma = 0.94$  and  $0.74 m\lambda$  for  $Z_9$  and  $Z_{16}$  respectively. For the other Zernike coefficients we found a reproducibility of about  $1m\lambda$  or better.

## 5. SUMMARY

In this paper we have discussed an aerial image based lens metrology method, the Extended Nijboer-Zernike method and its application to aberration measurement of a high-NA optical system of a wafer stepper. The ENZ-method is based on the observation of the through-focus intensity point-spread function of the projection lens. The mathematical framework was shown and the experimental procedure to extract aberrations for a high-NA lens is demonstrated on a high-NA DUV lithographic lens. The advantage of ENZ is a relatively simple set-up that may be operated with an incoherent light source. The method provides high reproducibility and a good match to the PMI. In addition, the ENZ-method determines not only the phase errors but also the transmission errors of the projection lens.

## ACKNOWLEDGMENTS

The authors wish to thank Hiroshi Ooki from Nikon Corporation, Japan and Martin McCallum from Nikon Precision, Europe as well as Yuri Aksenov from Philips Research Europe, Belgium for their helpful discussions.

## 6. APPENDIX

This appendix gives the definitions of the scaled coordinates as well as the definition of the  $V_n^m$ -functions for the low-NA case. In addition, we indicate how to modify the  $V_n^m$ -functions to the high-NA case of the experimental set-up, so that we *exactly* meet our experimental conditions.

The relationship between normalized image coordinates  $(x, y)$ , the defocus parameter  $f$  and the real space image coordinates  $(X, Y, Z)$  in the lateral and axial direction is given by:

$$x = X \frac{NA}{\lambda} \quad , \quad y = Y \frac{NA}{\lambda} \quad (9)$$

$$r = \sqrt{x^2 + y^2} \quad , \quad (x, y) = (r \cos \phi, r \sin \phi)$$

$$f = 2 \frac{\pi}{\lambda} Z(1 - \sqrt{1 - NA^2}) \quad ,$$

with  $(r, \phi)$  polar coordinates in the image plane.

The point-spread function or impulse response of an optical system is the image of an infinitely small object. In practice an object having a diameter of the order of  $\frac{\lambda}{2NA}$  is a fair approximation. The Extended Nijboer-Zernike theory is used to calculate the complex amplitude of the aberrated through-focus point-spread function. This calculation involves the  $V_n^m(r, f)$ -functions. For integers  $n, m \geq 0$  with  $n - m \geq 0$  and even, the Bessel series representation for  $V_n^m(r, f)$  reads

$$V_n^m(r, f) = \exp(ief) \sum_{l=1}^{\infty} (-2if)^{l-1} \sum_{j=0}^p v_{lj} \frac{J_{m+l+2j}(v)}{l^l} \quad , \quad (10)$$

with  $v = 2\pi r$ . The  $v_{lj}$  are given by

$$v_{lj} = (-1)^p (m+l+2j) \binom{m+j+l-1}{l-1} \binom{j+l-1}{l-1} \binom{l-1}{p-j} / \binom{q+l+j}{l} \quad , \quad (11)$$

where  $l = 1, 2, \dots$ ;  $j = 0, \dots, p$ . In Eq. 11 we have set

$$p = \frac{n-m}{2} \quad , \quad q = \frac{n+m}{2} \quad . \quad (12)$$

The effect of a non-negligible diameter is taken into account by modifying the focus parameter. For details we refer to Ref.<sup>10</sup>

The  $V_n^m(r, f)$ -functions are valid for an optical system with a low-to-medium-high NA value. However, the maximum NA-value of 0.78 of the experimental set-up requires a high-NA calculation. We note that defocus takes place on the high-NA side, i.e., at wafer level, but image formation occurs at the low-NA side of the CCD-camera. By replacing the scalar  $V_n^m(r, f)$ -functions of Eq. (10) by the  $V_{nm,j=0}$ -functions, arising from the vector calculation and removing the so-called radiometric effect from the calculation, we exactly meet our experimental conditions. For further details concerning the high-NA ENZ-theory of diffraction and aberration retrieval we refer to Ref.<sup>2</sup>

## REFERENCES

1. T. Matsuyama, I. Tanaka, T. Ozawa, K. Nomura, Takashi Koyama, "Improving lens performance through the most recent lens manufacturing process", Proc. SPIE **5040**, p. 801, (2003)
2. J.J.M. Braat, P. Dirksen, A.J.E.M. Janssen, S. van Haver, A.S. van de Nes, "Extended Nijboer-Zernike approach to aberration and birefringence retrieval in a high-numerical-aperture optical system", JOSA **A22**, p. 2635 (2005)
3. P. Dirksen, J.J.M. Braat, A.J.E.M. Janssen, A. Leeuwstein, "Aberration retrieval for high-NA optical systems using the Extended Nijboer-Zernike theory", Proc. SPIE **5754**, p. 262 (2005)
4. R. W. Gerchberg and W. O. Saxton, "Practical algorithm for determination of phase from image and diffraction pictures," Optik **35**, p. 237 (1972)
5. J. R. Fienup, J. C. Marron, T. J. Schultz, and J. H. Seldin, "Hubble space telescope characterized by using phaseretrieval algorithms", Appl. Opt. **32**, p. 1747 (1993)
6. J.P. Kirk, T.A. Brunner, "Measurement of microlithography aerial image quality", Proc. SPIE **2726**, p. 410 (1996)
7. F. Zach, C.Y. Lin, J.P. Kirk, "Aberration analysis using reconstructed aerial images of isolated contacts on attenuated phase-shift masks", Proc. SPIE **4346**, p. 1362 (2001)
8. M. Born and E. Wolf, *Principles of Optics* (4th rev. ed., Pergamon Press, New York, 1970), sec. 8.8

9. C. van der Avoort, J.J.M. Braat, P. Dirksen, A.J.E.M. Janssen, "Aberration retrieval from the intensity point-spread function in the focal region using the Extended Nijboer-Zernike approach", *J. Mod. Opt.* **52**, p. 1695 (2005)
10. P. Dirksen, J.J.M. Braat, A.J.E.M. Janssen, "Estimating resist parameters in optical lithography using the Extended Nijboer-Zernike theory", *accepted for publication* in *J. Microlith. Microfabr. Microsyst.*, 2006
11. See the Extended Nijboer-Zernike website: [www.nijboerzernike.nl](http://www.nijboerzernike.nl)